Acta Physica Polonica B Proceedings Supplement **17**, 5-A14 (2024)

PRODUCTION OF CHARM AND NEUTRINOS IN FAR-FORWARD EXPERIMENTS AT THE LHC*

Rafał Maciuła[a], Antoni Szczurek[a,b]

[a]Institute of Nuclear Physics Polish Academy of Sciences
Radzikowskiego 152, 31-342 Kraków, Poland
[b]College of Natural Sciences, Institute of Physics, University of Rzeszów
Pigonia 1, 35-310 Rzeszów, Poland

Received 24 April 2024, accepted 22 May 2024, published online 5 August 2024

We discuss far-forward production of charm mesons and neutrinos from their semileptonic decays in proton–proton collisions at the LHC energies. We include the gluon–gluon fusion $gg \to c\bar{c}$, the intrinsic charm (IC) $gc \to gc$ as well as the recombination $gq \to Dc$ partonic mechanisms. We present energy distributions for forward electron, muon, and tau neutrinos to be measured at the LHC by the FASERν experiment. For all kinds of neutrinos, the IC and the recombination dominate over the standard charm production contribution for neutrino energies $E_\nu > 300$ GeV. For electron and muon neutrinos, both mechanisms lead to a similar production rates and their separation seems rather impossible. On the other hand, for $\nu_\tau + \bar{\nu}_\tau$ neutrino flux, the recombination is reduced making the measurement of the IC contribution very attractive.

DOI:10.5506/APhysPolBSupp.17.5-A14

1. Introduction

The forward production of charm is not fully under control. There are some mechanisms which may play a role outside the mid-rapidity region (forward/backward production) not only at high-collision energies. There are potentially two QCD mechanisms that may play a role in this region: the mechanism of production of charm initiated by intrinsic charm which can be called knock-out of the intrinsic charm, and recombination of charm quarks/antiquarks and light antiquarks/quarks.

Recently, we have shown that at lower energies, the mechanisms easily mix and it is difficult to disentangle them in the backward production of D mesons [1]. Nevertheless, such fixed-target experiments provide some

* Presented at the 30$^{\text{th}}$ Cracow Epiphany Conference on *Precision Physics at High Energy Colliders*, Cracow, Poland, 8–12 January, 2024.

limitations on the not fully explored mechanisms. The asymmetry in the production of D^0 ($\bar{D}^0$) mesons may soon provide a piece of interesting information on the recombination mechanism. Some limitations on the intrinsic charm component were obtained recently based on the IceCube neutrino data [2].

In this paper, we will discuss far-forward production of charm at the LHC energies. The forward production of charm mesons leads to the forward production of neutrinos coming from their semileptonic decays. Recently, several new detectors were proposed to measure the forward neutrinos (*e.g.* FASERν, SND@LHC, FASERν2, FLArE) according to the Forward Physics Facility (FPF) proposal [3–5]. Here, we wish to summarize the situation for the collider mode of the LHC and try to answer whether such measurements can provide new interesting information on the poorly known mechanisms or not.

2. Details of the model calculations

In the present study, we take into consideration three different production mechanisms of charm, including:

(a) the standard (and usually considered as a leading) QCD mechanism of gluon–gluon fusion: $g^* g^* \to c\bar{c}$ with off-shell initial state partons, calculated both in the full k_{T}-factorization approach and in the hybrid model;

(b) the mechanism driven by the intrinsic charm component of proton: $g^* c \to gc$ calculated in the hybrid approach with off-shell initial-state gluon and collinear intrinsic charm distribution;

(c) the recombination mechanism: $gq \to Dc$ calculated in the leading-order collinear approach.

Calculations of the three contributions are performed following our previous studies reported in Refs. [1, 6–9].

2.1. The standard QCD mechanism for charm production

The standard QCD mechanism of gluon–gluon fusion for the $c\bar{c}$-pair production (see Fig. 1) is obtained within the hybrid model discussed by us in detail in Ref. [8]. The FPF experiments at the LHC will allow to explore the charm cross section in the far-forward rapidity direction where asymmetric kinematical configurations are selected. Thus, in the basic $gg \to c\bar{c}$ reaction both gluon PDFs are simultaneously probed at different longitudinal momentum fractions — extremely small for the gluon on the one side and very large for the gluon on the second side.

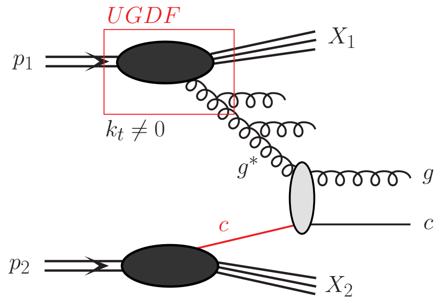

Fig. 1. A diagrammatic representation of the intrinsic charm driven mechanism of charm production within the hybrid model with the off-shell gluon and the on-shell charm quark in the initial state.

Within the asymmetric kinematic configuration $x_1 \ll x_2$, the cross section for the processes under consideration can be calculated in the so-called hybrid factorization model motivated by the work in Ref. [10]. In this framework, the small-x gluon is taken to be off-mass shell and the differential cross section *e.g.* for $pp \to c\bar{c}X$ via $g^*g \to c\bar{c}$ mechanism reads

$$\mathrm{d}\sigma_{pp\to c\bar{c}X} = \int \mathrm{d}^2k_t \int \frac{\mathrm{d}x_1}{x_1} \int \mathrm{d}x_2\, \mathcal{F}_{g^*}\left(x_1, k_t^2, \mu^2\right)\, g\left(x_2, \mu^2\right)\, \mathrm{d}\hat{\sigma}_{g^*g\to c\bar{c}}\,, \tag{1}$$

where $\mathcal{F}_{g^*}(x_1, k_t^2, \mu^2)$ is the unintegrated gluon distribution in one proton (gluon uPDF) and $g(x_2, \mu^2)$ a collinear PDF in the second one. The $\mathrm{d}\hat{\sigma}_{g^*g\to c\bar{c}}$ is the hard partonic cross section obtained from a gauge-invariant tree-level off-shell amplitude. A derivation of the hybrid factorization from the dilute limit of the Color Glass Condensate approach can be found *e.g.* in Ref. [11] (see also Ref. [12]). The relevant cross sections are calculated with the help of the KaTie Monte Carlo generator [13].

As a default set in the numerical calculations, we take the renormalization scale $\mu^2 = \mu_{\mathrm{R}}^2 = \sum_{i=1}^{n} \frac{m_{it}^2}{n}$ (averaged transverse mass of the given final state) and the charm quark mass $m_c = 1.5$ GeV. The strong-coupling constant $\alpha_{\mathrm{s}}(\mu_{\mathrm{R}}^2)$ at next-to-next-to-leading-order is taken from the CT14nnloIC PDF [14] routines.

2.2. The intrinsic charm induced component

The intrinsic charm contribution to charm production cross section (see Fig. 1) is also obtained within the hybrid approach. The differential cross section for $pp \to gcX$ via $g^*c \to gc$ mechanism reads

$$\mathrm{d}\sigma_{pp\to gcX} = \int \mathrm{d}^2k_t \int \frac{\mathrm{d}x_1}{x_1} \int \mathrm{d}x_2\, \mathcal{F}_{g^*}\left(x_1, k_t^2, \mu^2\right)\, c\left(x_2, \mu^2\right)\, \mathrm{d}\hat{\sigma}_{g^*c\to gc}\,, \tag{2}$$

where on large-x side instead of collinear gluon PDF we have $c(x_2, \mu^2)$ — a collinear charm quark PDF with intrinsic charm content. According to the KaTie approach, the initial-state quarks (including heavy quarks) can be treated as massless partons only. So here, we are limited to the massless formalism. Working with minijets (jets with transverse momentum of the order of a few GeV) requires a phenomenologically motivated regularization of the cross sections. Here, we follow the minijet model [15] adopted *e.g.* in PYTHIA Monte Carlo generator, where a special suppression factor is introduced at the cross section level [16]

$$F(p_{\mathrm{t}}) = \frac{p_{\mathrm{t}}^2}{p_{\mathrm{T0}}^2 + p_{\mathrm{t}}^2} \tag{3}$$

for each of the outgoing massless partons with transverse momentum p_{t}, where p_{T0} is a free parameter of the form factor that also enters as an argument of the strong coupling constant $\alpha_{\mathrm{S}}(p_{\mathrm{T0}}^2 + \mu_{\mathrm{R}}^2)$. A phenomenological motivation behind its application in the k_{T}-factorization approach is discussed in detail in Ref. [17].

In the numerical calculations below, the intrinsic charm PDFs are taken at the initial scale $m_c = 1.3$ GeV, so the perturbative charm contribution is intentionally not taken into account. We apply different grids of the intrinsic charm distribution from the CT14nnloIC PDF [14].

2.3. Recombination model of charmed meson production

The underlying mechanism of the Braaten–Jia–Mechen (BJM) [18–20] recombination is illustrated in Fig. 2. Differential cross section for production of Dc final state can be written as

$$\begin{aligned}\frac{\mathrm{d}\sigma}{\mathrm{d}y_1\,\mathrm{d}y_2\,\mathrm{d}^2p_{\mathrm{t}}} = \frac{1}{16\pi^2\hat{s}^2}\Big[& x_1 q_1\left(x_1,\mu^2\right)\, x_2 g_2\left(x_2,\mu^2\right)\overline{|\mathcal{M}_{qg\to Dc}(s,t,u)|^2} \\ &+ x_1 g_1\left(x_1,\mu^2\right)\, x_2 q_2\left(x_2,\mu^2\right)\overline{|\mathcal{M}_{gq\to Dc}(s,t,u)|^2}\Big]\,. \end{aligned} \tag{4}$$

Above, y_1 is rapidity of the D meson and y_2 rapidity of the associated c or $\bar{c}$.

The matrix element squared in (4) reads

$$\overline{|\mathcal{M}_{qg\to Dc}(s,t,u)|^2} = \overline{|\mathcal{M}_{qg\to(\bar{c}q)^n c}|^2}\,\rho\,, \tag{5}$$

where n enumerates quantum numbers of the $\bar{c}q$ system $n \equiv {}^{2J+1}L$ and ρ can be interpreted as a probability to form real meson. For illustration as our default set, we shall take $\rho = 0.1$, but the precise number should be adjusted to experimental data. For the discussion of the parameter, see *e.g.* Refs. [19, 20] and references therein. The asymmetries observed in

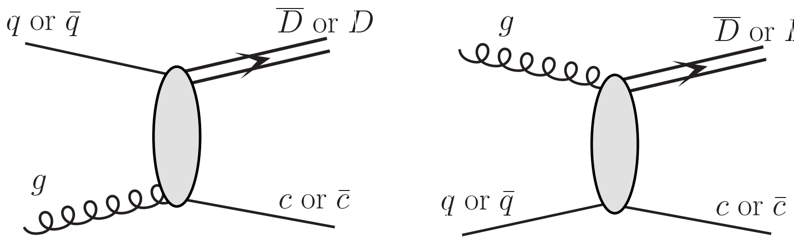

Fig. 2. Generic leading-order diagrams for D meson production via the BJM recombination.

photoproduction can be explained with $\rho = 0.15$ [20]. Some constrains for this parameter were also presented from the LHCb fixed-target data on D-meson production asymmetry [1].

The explicit form of the matrix element squared can be found in [18] for pseudoscalar and vector-meson production for color singlet and color octet meson-like states. A similar formula can be written for production of $\bar{D}\bar{c}$. Then, the quark distribution is replaced by the antiquark distribution. In the following, we include only color singlet $(q\bar{c})^n$ or $(\bar{q}c)^n$ components. As a default set, the factorization scale in the calculation is taken as

$$\mu^2 = p_{\mathrm{t}}^2 + \frac{m_{\mathrm{t},D}^2 + m_{\mathrm{t},c}^2}{2} \,. \tag{6}$$

Within the recombination mechanism, we include fragmentation of c-quarks or $\bar{c}$-antiquarks accompanying directly produced D-mesons or $\bar{D}$-antimesons, *e.g.*

$$\mathrm{d}\sigma \left[qg \to \bar{D}_{\mathrm{direct}} + D_{\mathrm{frag}}\right] = \mathrm{d}\sigma \left[qg \to \bar{D} + c\right] \otimes F_{c\to D}^{\mathrm{frag}} \,, \tag{7}$$

where $F_{c\to D}^{\mathrm{frag}}$ is the relevant fragmentation function.

2.4. Hadronization of charm quarks

The transition of charm quarks to open charm mesons is done in the framework of the independent parton fragmentation picture (see *e.g.* Ref. [21]) where the inclusive distributions of open charm meson can be obtained through a convolution of inclusive distributions of produced charm quarks and $c \to D$ fragmentation functions. Here, we follow exactly the method which was applied by us in our previous study of forward/backward charm production reported *e.g.* in Ref. [9]. According to this approach, we assume that the D meson is emitted in the direction of parent c-quark/antiquark, *i.e.* $\eta_D = \eta_c$ (the same pseudorapidities or polar angles) and the z-scaling variable is defined with the light-cone momentum *i.e.* $p_c^+ = \frac{p_D^+}{z}$, where $p^+ = E + p$. In numerical calculations, we take the Peterson fragmentation function [22] with $\varepsilon = 0.05$, often used in the context of hadronization of heavy flavours.

2.5. Production of ν_e and ν_μ neutrinos

There are different sources of neutrinos (see [23]). In general, the ν_e neutrinos can be produced from the decays of K^+ and K_{L} mesons and the ν_μ neutrinos from K^+, K_{L}, and π^+. In addition both of them can be also produced from D^+, D^0, D_s^+ mesons via many decay channels. In the present study we are particularly interested in D-meson semileptonic decays. As will be discussed below we have no such decay functions. In practical evaluation, often a simplified decay function for kaon decays [24] is used also to the decays of charm mesons.

An alternative way to incorporate semileptonic decays into theoretical model is to take relevant experimental input. Here, we follow the method described in Refs. [25–27]. For example, the CLEO Collaboration [28] has measured very precisely the momentum spectrum of electrons/positrons coming from the decays of D mesons.

2.6. Production of ν_τ neutrino

The production mechanism of ν_τ or $\bar{\nu}_\tau$ is a bit more complicated. The decay of D_s mesons to ν_e and ν_μ is often neglected as the relevant $c \to D_s$ fragmentation fraction is relatively small $\mathrm{BR}(c \to D_s) \approx 8\%$ and further decay branching fractions to ν_e and ν_μ are about 2% only. On the other hand, the D_s mesons are quite unique in the production of ν_τ, in particular, decay of D_s mesons is the dominant mechanism of ν_τ production.

There are two mechanisms described shortly below: the direct decay mode: $D_s^+ \to \tau^+ \nu_\tau$ with $\mathrm{BR} = 5.32 \pm 0.11\%$ and the chain decay mode: $D_s^+ \to \tau^+ \to \bar{\nu}_\tau$. More information can be found in Ref. [30] dedicated to the SHIP fixed-target experiment where the production of the ν_τ neutrinos in a fixed-target $p + {}^{96}\mathrm{Mo}$ reaction at $\sqrt{s} = 27.4$ GeV was discussed.

The considered here decay channels: $D_s^+ \to \tau^+ \nu_\tau$ and $D_s^- \to \tau^- \bar{\nu}_\tau$, which are the sources of the direct neutrinos, are analogous to the standard text book cases of $\pi^+ \to \mu^+ \nu_\mu$ and $\pi^- \to \mu^- \bar{\nu}_\mu$ decays, discussed in detail in the past (see *e.g.* Ref. [31]). The same formalism used for the pion decay applies also to the D_s meson decays. As it was explicitly shown in Ref. [30], the τ lepton takes almost the whole energy of the mother D_s meson. This is because of the very similar mass of both particles: $m_\tau = 1.777$ GeV and $m_{D_s} = 1.968$ GeV. The direct neutrinos take only a small part of the energy and therefore will form the low-energy component of the neutrino flux observed by the FASERν experiment.

The τ decays are rather complicated due to having many possible decay channels [23]. Nevertheless, all confirmed decays lead to production of ν_τ $(\bar{\nu}_\tau)$. In the numerical calculations of ν_τ neutrinos/antineutrinos, we use a sample of 10^5 decays generated before by the dedicated TAUOLA program [36].

3. Numerical results

Now, we proceed to neutrino/antineutrino production. In Fig. 3, we show the energy distribution of $\nu_e + \bar{\nu}_e$ calculated for the $\sqrt{s} = 13$ TeV including the designed psuedorapidity acceptance $\eta > 8.5$ of the FASERν experiment. Here and in the following, the numbers of neutrinos are obtained for the integrated luminosity $L_{\text{int}} = 150$ fb^{-1}. In addition to the production from the semileptonic decays of D mesons, we show a contribution from the decay of kaons (dotted line) taken from [37]. The gluon–gluon fusion contribution is quite small, visibly smaller than the kaon contribution. Both the IC and recombination contributions may be seen as an enhancement over the contribution due to conventional kaons in the neutrino energy distribution at neutrino energies $E_\nu > 1$ TeV, however, the size of the effect is rather small. An identification of the subleading contributions will require a detailed comparison to the FASERν data. Here, the recombination and IC contributions may be of a similar order.

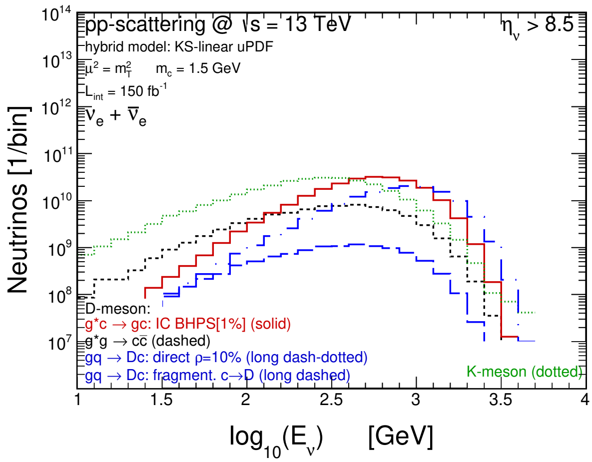

Fig. 3. Energy distribution of electron neutrinos+antineutrinos for $\eta > 8.5$ (FASERν).

The situation for muon neutrinos (see Fig. 4) is much more difficult as here a large conventional contribution from charged pion decays enters [37]. Here, the IC and recombination contributions are covered by the $\pi \to \nu_\mu$ (dot-dot-dashed), $K \to \nu_\mu$ (dotted) contributions even at large neutrino energies.

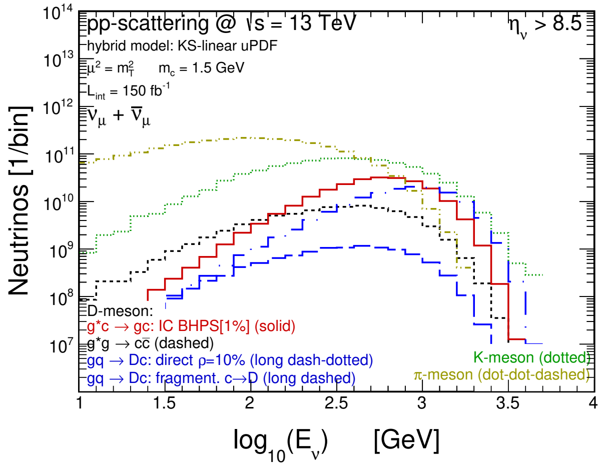

Fig. 4. Energy distribution of muon neutrinos+antineutrinos for $\eta > 8.5$ (FASERν).

Another option to identify the subleading contributions is to investigate energy distributions of ν_τ neutrinos which are, however, difficult to measure experimentally. Such distributions are shown in Fig. 5. Here again, the contribution of subleading mechanisms dominates over the traditional gluon–

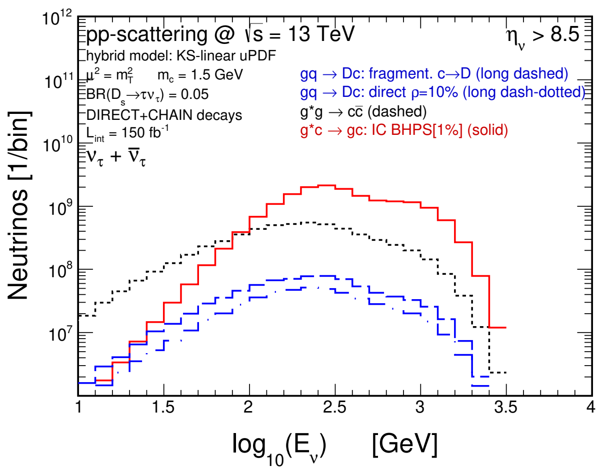

Fig. 5. Energy distribution of tau neutrinos+antineutrinos for $\eta > 8.5$ (FASERν).

gluon fusion mechanism. In addition, there is no contribution of light mesons due to limited phase space for τ production in the D_s decay. In this case, the contribution due to recombination is small compared to the electron and muon neutrinos case because $s(x) \ll u_{\rm val}(x), d_{\rm val}(x)$. Therefore, the measurement of ν_τ and/or $\bar{\nu}_\tau$ seems optimal to pin down the IC contribution in the nucleon.

REFERENCES

[1] R. Maciuła, A. Szczurek, *Phys. Lett. B* **835**, 137530 (2022), arXiv:2206.02750 [hep-ph].

[2] V.P. Goncalves, R. Maciuła, A. Szczurek, *Eur. Phys. J. C* **82**, 236 (2022).

[3] L.A. Anchordoqui *et al.*, *Phys. Rep.* **968**, 1 (2022).

[4] FASER Collaboration (H. Abreu *et al.*), *Eur. Phys. J. C* **80**, 61 (2020).

[5] SND@LHC Collaboration (G. Acampora *et al.*), *J. Instrum.* **19**, P05067 (2024), arXiv:2210.02784 [hep-ex].

[6] R. Maciuła, A. Szczurek, *Phys. Rev. D* **100**, 054001 (2019).

[7] R. Maciuła, *Phys. Rev. D* **102**, 014028 (2020).

[8] R. Maciuła, A. Szczurek, *J. High Energy Phys.* **2020**, 135 (2020).

[9] R. Maciuła, A. Szczurek, *Phys. Rev. D* **105**, 014001 (2022).

[10] M. Deak, F. Hautmann, H. Jung, K. Kutak, *J. High Energy Phys.* **2009**, 121 (2009).

[11] A. Dumitru, A. Hayashigaki, J. Jalilian-Marian, *Nucl. Phys. A* **765**, 464 (2006).

[12] P. Kotko *et al.*, *J. High Energy Phys.* **2015**, 106 (2015).

[13] A. van Hameren, *Comput. Phys. Commun.* **224**, 371 (2018).

[14] T.J. Hou *et al.*, *J. High Energy Phys.* **2018**, 059 (2018).

[15] T. Sjöstrand, M. van Zijl, *Phys. Rev. D* **36**, 2019 (1987).

[16] T. Sjöstrand *et al.*, *Comput. Phys. Commun.* **191**, 159 (2015).

[17] P. Kotko, A.M. Stasto, M. Strikman, *Phys. Rev. D* **95**, 054009 (2017).

[18] E. Braaten, Y. Jia, T. Mehen, *Phys. Rev. D* **66**, 034003 (2002).

[19] E. Braaten, Y. Jia, T. Mehen, *Phys. Rev. Lett.* **89**, 122002 (2002).

[20] E. Braaten, Y. Jia, T. Mehen, *Phys. Rev. D* **66**, 014003 (2002).

[21] R. Maciuła, A. Szczurek, *J. Phys. G: Nucl. Part. Phys.* **47**, 035001 (2020).

[22] C. Peterson, D. Schlatter, I. Schmitt, P.M. Zerwas, *Phys. Rev. D* **27**, 105 (1983).

[23] Particle Data Group (R.L. Workman *et al.*), *Prog. Theor. Exp. Phys.* **2022**, 083C01 (2022).

[24] P. Lipari, *Astropart. Phys.* **1**, 195 (1993).

[25] M. Łuszczak, R. Maciuła, A. Szczurek, *Phys. Rev. D* **79**, 034009 (2009).

[26] R. Maciuła, A. Szczurek, M. Łuszczak, *Phys. Rev. D* **92**, 054006 (2015).

[27] P. Bolzoni, G. Kramer, *Nucl. Phys. B* **872**, 253 (2013); *Erratum ibid.* **876**, 334 (2013).

[28] CLEO Collaboration (N.E. Adam *et al.*), *Phys. Rev. Lett.* **97**, 251801 (2006).

[29] ALICE COllaboration (B.B. Abelev *et al.*), *Phys. Rev. D* **91**, 012001 (2015).

[30] R. Maciuła, A. Szczurek, J. Zaremba, I. Babiarz, *J. High Energy Phys.* **2020**, 116 (2020).

[31] P. Renton, «Electroweak Interactions: An Introduction to the Physics of Quarks and Leptons», *Cambridge University Press*, Cambridge, UK 1990.

[32] T.K. Gaisser, «Cosmic Rays and Particle Physics», *Cambridge University Press*, Cambridge, UK 1990.

[33] S.M. Barr, T.K. Gaisser, P. Lipari, S. Tilav, *Phys. Lett. B* **214**, 147 (1988).

[34] L. Pasquali, M.H. Reno, *Phys. Rev. D* **59**, 093003 (1999).

[35] M. Artuso, B. Meadows, A.A. Petrov, *Annu. Rev. Nucl. Part. Sci.* **58**, 249 (2008).

[36] S. Jadach, J.H. Kühn, Z. Wąs, *Comput. Phys. Commun.* **64**, 275 (1990).

[37] F. Kling, L.J. Nevay, *Phys. Rev. D* **104**, 113008 (2021).